

Supporting Information towards:

Water mediated Proton Conduction in a Sulfonated Microporous Organic Polymer

C. Klumpen^a, S. Gödrich^b, G. Papastavrou^b, J. Senker^{a*}

^aUniversity of Bayreuth, Inorganic Chemistry III, Universitaetsstraße 30, 95447 Bayreuth, Germany

^bUniversity of Bayreuth, Physical Chemistry II, Universitaetsstraße 30, 95447 Bayreuth, Germany

Tables of Content

1. Experimental Section	3
1.1 General Information	3
1.2 Synthesis	6
1.2.1 Chemicals	6
1.2.2 Tetraphenylmethane ^[2]	6
1.2.3 Tetrakis(4-bromophenyl)methane ^[3]	7
1.2.4 PAF-1 ^[4]	8
1.2.5 SPAF-1(0.5) ^[4]	8
1.2.6 SPAF-1(1.25).....	9
2. Analytical Section	10
2.1 Linker analytics	10
2.1.1 Liquid NMR.....	10
2.1.1.1 ¹ H Tetraphenylmethane	10
2.1.1.2 ¹³ C Tetraphenylmethane	10
2.1.1.3 ¹ H Tetrakis(4-bromophenyl)methane	11
2.1.1.4 ¹³ C Tetrakis(4-bromophenyl)methane.....	11
2.1.2 Infrared spectroscopy	12
2.1.3 CHN-Analysis.....	12
2.1.3.1 Tetraphenylmethane	12
2.1.3.2 Tetrakis(4-bromophenyl)methane.....	13
2.2 Polymer analytics.....	13
2.2.1 Solid state NMR.....	13
2.2.1.1 ¹³ C_PAF-1.....	13
2.2.1.2 ¹³ C_SPAF-10.5.....	15

2.2.1.3 ^{13}C _SPAF-1(1.25)	15
2.2.2 Infrared spectroscopy	16
2.2.3 CHN-Analysis.....	16
2.2.3.1 PAF-1	16
2.2.3.2 SPAF-1(0.5).....	17
2.2.3.3 SPAF-1(1.25).....	17
2.2.4 Gas adsorption analysis – N_2 at 77K.....	17
2.2.4.1 PAF-1	17
2.2.4.2 SPAF-1(0.5).....	18
2.2.4.3 SPAF-1(1.25).....	19
2.2.5 Gas adsorption analysis – CO_2 at 273 K	20
2.2.5.1 PAF-1	20
2.2.5.2 SPAF-1(0.5).....	21
2.2.5.3 SPAF-1(1.25).....	21
2.2.5.4 Summary of gas sorption analysis	21
2.2.6 TGA analysis	22
2.2.6.1 Stability.....	22
2.2.6.2 Water Uptake	22
2.2.7 UV-Vis spectroscopy	23
2.2.8 Powder X-ray diffraction.....	23
2.2.9 Impedance spectroscopy.....	24
2.2.9.1 PAF-1(0.5).....	24
50 % rH (K_2CO_3):.....	24
30 % rH ($\text{H}_3\text{C}_2\text{OOK}$):.....	25
2.2.9.2 SPAF-1(1.25).....	26
50 % rH (K_2CO_3):.....	26
30 % rH ($\text{H}_3\text{C}_2\text{OOK}$):.....	27
2.2.10 Differential scanning calorimetry	28
2.2.11 Energy dispersive X-ray spectroscopy	29
2.2.12 Atomic force microscopy	30
3. Literature	31

1. Experimental Section

1.1 General Information

Nitrogen sorption measurements were carried out on a Quantachrome Autosorb-1 pore analyzer at 77 K. The data were analyzed using the ASIQ v 3.0 software package. Pore size distributions were calculated with methods of quasistationary density functional theory (QSDFT). CO₂ adsorption isotherms were measured on a Quantachrome Nova surface analyzer at 273 K. Based on these, calculations of the specific surface area, pore volumes and pore size distributions were carried out using the nonlocal density functional theory (NLDFT) slit-pore model for carbon materials. For the N₂-based isotherms, the N₂ at 77 K on Carbon (slit/cylindr. pores QSDFT adsorption branch) kernel was used. All polymers were degassed at 150 °C for 12 h before starting the sorption experiments.

¹H and ¹³C liquid-NMR spectra of the linker molecules were collected on a Bruker 500 MHz spectrometer using DMSO as solvent. For infrared spectra (IR) a JASCO FT/IR-6100 Fourier transform infrared spectrometer with an attenuated total reflectance (ATR) unit was used. CHN analysis was carried out at a vario EL-III with acetanilide as standard (Measured: C [71.09], H [6.71], N [10.36]. Calcd: C [71.09], H [6.71], N [10.36]). Mass spectrometry (MS) was performed at a Finnigan MAT-8500-spectrometer with an ionization energy of 70 eV. Thermogravimetric analysis (TGA) was carried out on a Mettler Toledo TGA/SDTA851^e under air. Powder X-ray diffraction (PXRD) measurements were performed on a PANalytical X'Pert Pro diffractometer. Here, a region from 2 to 30° 2θ was measured with a 1/4 antiscatter slit and Cu K_α radiation (nickel filtered). For the titration experiments a *Mettler Toledo* pH meter has been used with an aqueous NaOH solution as reference. UV-Vis experiments were performed on a *Varian Cary 300 Scan* UV-Visible spectrometer using an Ulbricht sphere.

All solid-state NMR spectra were acquired on a Bruker Avance III HD spectrometer operating at a B₀ field of 9.4 T. ¹³C (δ = 100.6 MHz) MAS spectra were obtained with ramped cross-polarization (CP) experiments where the nutation frequency ν_{nut} on the proton channel was varied linearly from 70 – 100 %. The samples were spun at 12.5 kHz (¹³C) in a 4 mm MAS double resonance probe (Bruker). The corresponding ν_{nut} on the ¹³C channel and the contact time were adjusted to 70 kHz and 3.0 ms, respectively. Proton broadband decoupling with spinal-64 and $\nu_{\text{nut}} = 12.5$ kHz was applied during acquisition.^[1] ¹³C spectra are referenced with respect to TMS (tetramethylsilane) using the secondary standard adamantane. Quantitative single pulse experiments were carried out with a 90° pulse with a length of 3.70 μs and a recycle delay of 120 s.

For EDX measurements the sample was prepared as is on a stub with double sided sticky carbon tape and then coated with 20 nm carbon using a Leica EM ACE600 carbon coater. The EDS analysis was performed in a FEI Quanta FEG 250 Scanning Electron Microscope (SEM) under low vacuum conditions (45 Pa) with a SDD detector from Thermo Fisher Scientific applying an accelerating voltage of 5 kV. (Images were taken with a Large Field Detector (LFD) for secondary electrons and a Concentric Back Scattered Detector (CBS) for backscattered electrons.) To exclude microphase separation within the polymers at high relative humidities, we exchanged the hydrogens of the $-\text{SO}_3\text{H}$ units with sodium. Therefore, the material was stirred in saturated NaCl solution for 24 h including an exchange of the salt solution. The material was then dried in vacuo at 100 °C for 12 h and sputtered with carbon before performing the EDX experiment. For a phase separating material we expected concentrated regions for sodium due to an eased access into the network.

The crystallization temperatures of the sample were determined using a Mettler Toledo DSC/SDTA 821e DSC with autosampler. The measurements were performed over a temperature range of -80 °C - 120 °C at a heating/cooling rate of 2 °C/min under nitrogen atmosphere. Prior measurements, SPAF-1(1.25) was saturated at 30 % and 100 % rH for 24 hours, respectively.

Atomic force microscopy measurements were performed on a SPAF-1(1.25)-pellet, which was prepared from moist SPAF-1(1.25)-powder using a hand-held pill press. The sample was directly measured on the copper block of the press, which was placed in a petri-dish filled with water in order to prevent the sample from drying. The sample was imaged using tapping mode in air on Dimension ICON (Bruker) with a OTESPA-R3 cantilever (Olympus). Height images (Figure S27 left) at different sample spots show a granular morphology of the compressed powder material.

Impedance spectroscopy was carried out on a Zahner (Z) Emium potentiostat with an applied perturbation voltage of 10 mV. An impedance data set was created measuring the frequency range from from 1 MHz to 100 mHz. To ensure the shape and size of the pellet remains equal during the whole measuring procedure, the material was placed into a cylindrical bordering. The resulting pellets were placed between two copper electrodes and stored under defined humidity, obtained by saturated salt solutions, at 20 °C for 24 h (Table S1). To ensure equilibration before the measurements, an equilibration time of 30 minutes was included into the measurement protocol. After performing the measurements the length (l) and radius (r)

($A=r^2 \cdot \pi$) of the pellet have been taken and the conductivity was calculated using following equation:

$$\kappa = \frac{l}{(A \cdot R2)}$$

Were the resistance (R) was taken from the high frequency semicircle in the appropriate Nyquist plot (Cole-Cole plot), which has been fitted with an optimized Randles-Cell (Figure 3, top) using Zview (Scribner).

Table S1. Saturated salt solutions to obtain a defined relative humidity during EIS and TGA analysis.

Salt	Relative Humidity / %
vacuum	0
$K^+(H_3C_2O_2)^-$	30
K_2CO_3	50
$NaNO_3$	70
KCl	80
H_2O	100

1.2 Synthesis

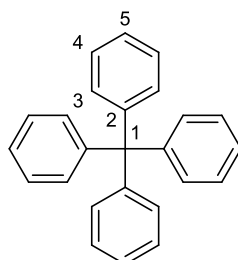
All chemicals were purchased at *Sigma-Aldrich Chemistry GmbH*, *VWR Chemicals*, *TCI* or *Grüssing* and, if not mentioned otherwise, were used without further purification (Tab. S2). All polymerizations were carried out under argon atmosphere in dry vessels. DMF and THF were purchased as technical reagents and purified via distillation.

1.2.1 Chemicals

Table S2: List of chemicals used for this publication, their purities and distributor.

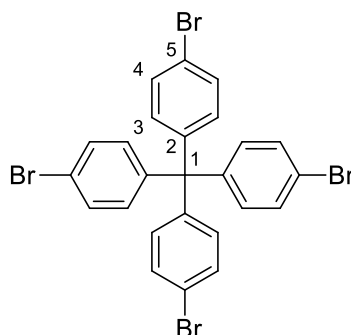
Chemical	Company	Purity
Aniline	Sigma Aldrich	>99.5 %
Brom	Sigma Aldrich	99.99 %
Chlorosulfonic acid	Merck-Millipore	-
2,5-Cyclooctadien	Sigma Aldrich	> 99 %
Dichloromethan	VWR-Chemicals	99.9 %
Dimethylformamide	VWR-Chemicals	>99.8 %
Ethanol	VWR-Chemicals	>96 %
Isopentylnitrite	Sigma Aldrich	96 %
Ni(cod) ₂	Sigma Aldrich	-
Phosphinic acid sol.	Sigma Aldrich	50 wt % in H ₂ O
Sulfuric acid fuming	Merck-Millipore	65 % SO ₃
Tetrahydrofuran	VWR-Chemicals	-
Triphenylchloromethane		
K ₂ CO ₃	Sigma Aldrich	97%
NaNO ₃	Sigma Aldrich	> 99 %
KCl	Sigma Aldrich	> 99 %
H ₃ C ₂ OOK	Sigma Aldrich	> 99 %
Sulfuric acid fuming	Merck-Millipore	65 % SO ₃

1.2.2 Tetraphenylmethane^[2]



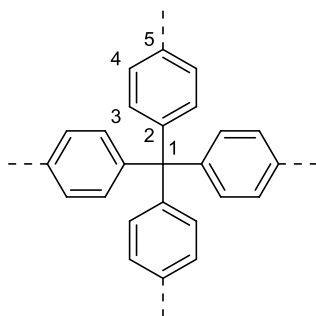
15 g of trityl chloride (0.054 mol, 1 eq.) and 14.05 ml aniline (0.154 mol, 2.9 eq.) were heated up to 180 °C in a round flask with magnetic stirrer and condenser, until the reaction mixture turned into a violet solid. The heating process was extended for 10 more minutes. The solid was cooled down, crushed and resuspended in 75 ml MeOH and 75 ml 2 M HCl. The Suspension was refluxed for 30 min., filtered and washed with water. After resuspending in ethanol the reaction mixture was cooled down to -30 °C and 15.75 ml sulfuric acid and 9.44 g of isopentyl nitrite (0.081 mol, 1.5 eq.) were added under vigorous stirring. After stirring for 1 h at -10 °C, 26.9 ml of phosphinic acid (0.609 mol, 11 eq.) were added slowly and the reaction mixture was refluxed for 1.5 h. After cooling down, the solid was filtered, washed with DMF, H₂O and Ethanol and subsequently dried *in vacuo* to get a light brown powder. Further purification was not necessary but could be done by recrystallization in THF/methanol (1:1). Yield: 16.1 g (0.05 mol, 93 %). ¹H-NMR (500 MHz, DMSO-D₆): δ [ppm] = 7.30 (t, 1H, H-4), 7.21 (t, 1H, H-5), 7.15 (d, 1H, H-3) (Fig. S3). ¹³C-NMR (500 MHz, DMSO-D₆): δ [ppm] = 146.88 (C-2), 130.94 (C-3), 128.19 (C-4), 126.44 (C-5) (Fig. S4). EA [%]: C [91.25], H [6.54], N [0.18]; Calc.: C [93.71], H [6.29], N [0.00]. MS [M/z] = 243, 320, 165. IR (ATR): ν [cm⁻¹] = 1590, 1490, 1181, 1072, 1034, 767, 750, 696, 629, 491 (Fig. S7).

1.2.3 Tetrakis(4-bromophenyl)methane^[3]



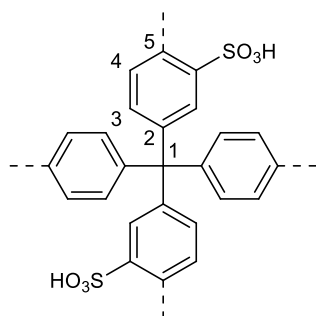
In a three necked vessel with magnetic stirrer, thermometer and condenser 10 g tetraphenylmethane (31.2 mmol, 1 eq.) were cooled in an ice bath. Now 99.75 g Br₂ (624 mmol, 20 eq.) were added dropwise. After cooling towards -78 °C, 140 ethanol (4.5 ml/mmol) were applied and the mixture was allowed to reach room temperature overnight. Now sodiumdisulfide solution was added until the end of precipitation. The resulting solid was filtered, washed with H₂O and dried in an oven at 110 °C. Further purification was carried out performing recrystallization in a chloroform/ethanol mixture (1:1) to get a light brown solid. Yield: 12.9 g (20.28 mmol, 65 %). ¹H-NMR (500 MHz, DMSO-D₆): δ [ppm] = 7.53 (d, 2H, H-4), 7.06 (d, 2H, H-3) (Fig. S5). ¹³C-NMR (500 MHz, DMSO-D₆): δ [ppm] = 63.66 (C-1), 120.40 (C-5), 131.55 (C-3), 132.86 (C-4), 145.06 (C-2) (Fig. S6). EA [%]: C [46.09], H [2.13]; Calc.: C [47.21], H [2.54]. MS [M/z] = 279, 239, 636, 319, 555, 198. IR (ATR): ν [cm⁻¹] = 1569, 1486, 1393, 1181, 1072, 1005, 951, 908, 808, 750, 528, 507 (Fig. S7).

1.2.4 PAF-1^[4]



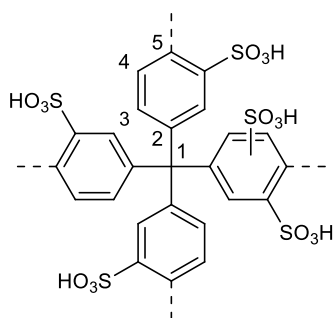
80 ml DMF_{dry} (21 ml/mmol), 1.14 g 2,2-bipyridiyl (7.29 mmol, 1 eq.), 2 g Ni(cod)₂ (7.27 mmol, 1 eq.), 0.8 ml cyclooctadiene (8.4 mmol, 1.2 eq.), 80 ml THF_{dry} (21 ml/mmol) and 1.16 g tetrakis(4-bromophenyl)methane (1.82 mmol, 0.22 eq.) were placed in a dry vessel under Ar and stirred for 9 h at room temperature. The mixture was cooled to 0 °C and 50 mL 6 M HCl were added dropwise and stirred overnight (13 h). The resulting solid was filtered, washed with MeOH. Further purification was done via a soxhlett apparatus with MeOH/THF (1:1) for 5 h. Yield: 0.458 g (1.45 mmol; 80 %). ¹³C NMR (CP-MAS, 12.5 kHz): δ [ppm] = 64.6 (C-1), 125.3 (C-3), 139, 34 (C-5), 145.9 (C-2) (Fig. S8). EA [%]: C [92.17], H [5.738], N [0.632]; Calc.: C [94.9], H [5.1], N [0.00]. IR (ATR): ν [cm⁻¹] = 3079, 3059, 3031, 1601, 1547, 1482, 1439, 1395, 1265, 1189, 1113, 1069, 1037, 1004, 961, 917, 839, 748, 701, 650, 630, 524 (Fig. S11).

1.2.5 SPAF-1(0.5)^[4]



100 mg ($3.16 \cdot 10^{-4}$ mol, 1 eq.) PAF-1 were suspended in 50 ml dichloromethane and cooled down to 0 °C. After dropwise addition of 0.11 ml ($1.58 \cdot 10^{-3}$ mol, 5 eq) chlorosulfonic acid, the suspension was stirred for 3 days at room temperature. The mixture was poured into ice and the solid was filtered, washed with H₂O and dried in vacuum to obtain a violet powder. Yield: 0.124 g ($2.60 \cdot 10^{-4}$ mol, >82 %). ¹³C NMR (CP-MAS, 12.5 kHz): δ [ppm] = 149-143 (2,5), 141-135 (3'), 132-126 (3,4,5'), 64 (1) (Fig. S9). EA [%]: C [65.47], H [4.45], N [0.47]; Calc.: C [63.01], H [3.38], N [0.00]. IR (ATR): ν [cm⁻¹] = 3500-2500, 3032, 2919, 2855, 1682, 1596, 1578, 1486, 1356, 1283, 1176, 1130, 1096, 1037, 1001, 898, 815, 745, 711, 606, 562, 539 (Fig. S11).

1.2.6 SPAF-1(1.25)



100 mg ($3.16 \cdot 10^{-4}$ mol, 1 eq.) of PAF-1 were activated at 150 °C in vacuum for 2 h. Now fuming sulfuric acid (65 % SO₃) was applied via gas phase for 10 minutes (Figure SNumber). The resulting solid was dried in vacuum at 150 °C for 1 h to yield a deep purple powder. Yield: 235 mg ($3.28 \cdot 10^{-4}$ mol, >99 %). ¹³C NMR (CP-MAS, 12.5 kHz): δ [ppm] = 65.8 (C-1), 123.5 (C-6), 130, 3 (C-7), 147.8 (C-2/4) (Fig. S10). EA [%]: C [41.31], H [3.71], N [0.53]; Calc.: C [41.90], H [2.25], N [0.00]. IR (ATR): ν [cm⁻¹] = 3500-2500, 1687, 1589, 1489, 1468, 1468, 1354, 1291, 1266, 1169, 1127, 1090, 1039, 1001, 938, 888, 825, 750, 712, 556, 507, 457 (Fig. S11).

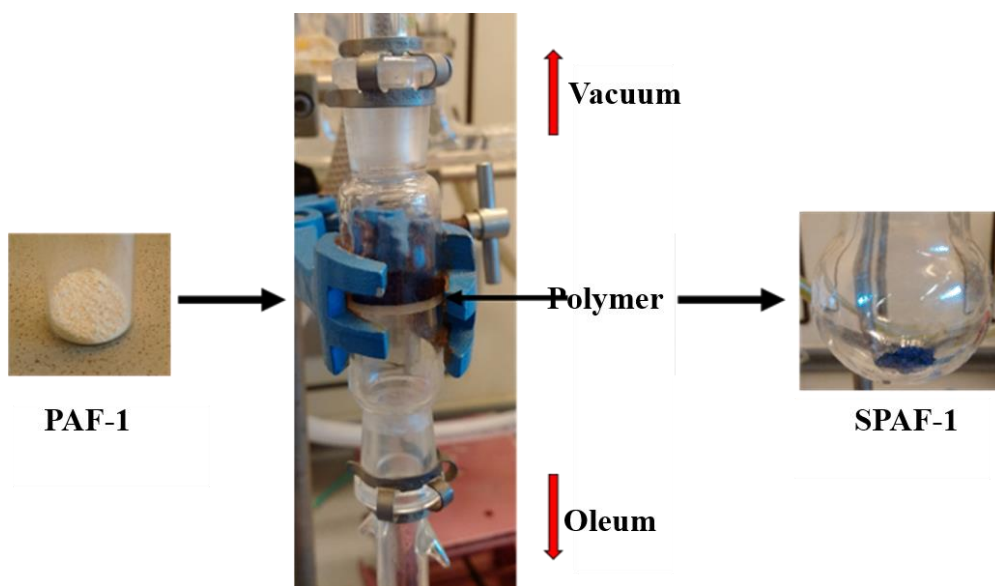


Figure S1: Schematic presentation of the gas phase sulfonation concept.

2. Analytical Section

2.1 Linker analytics

2.1.1 Liquid NMR

2.1.1.1 ^1H Tetraphenylmethane

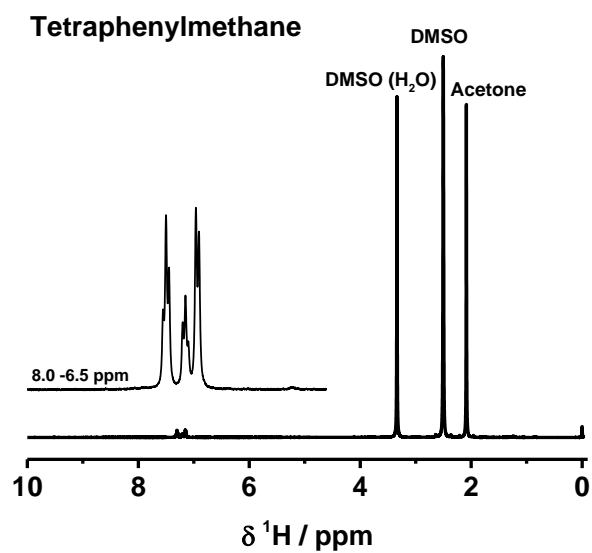


Figure S2: ^1H liquid NMR spectra of Tetraphenylmethane.

2.1.1.2 ^{13}C Tetraphenylmethane

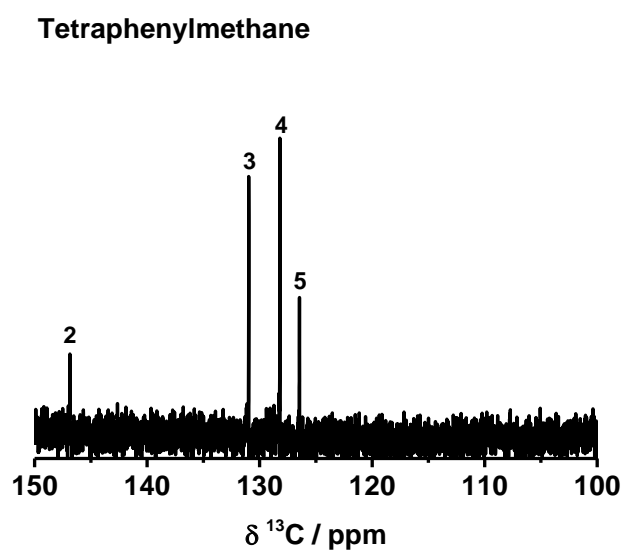


Figure S3: ^{13}C liquid NMR spectra of Tetraphenylmethane.

2.1.1.3 ^1H Tetrakis(4-bromophenyl)methane

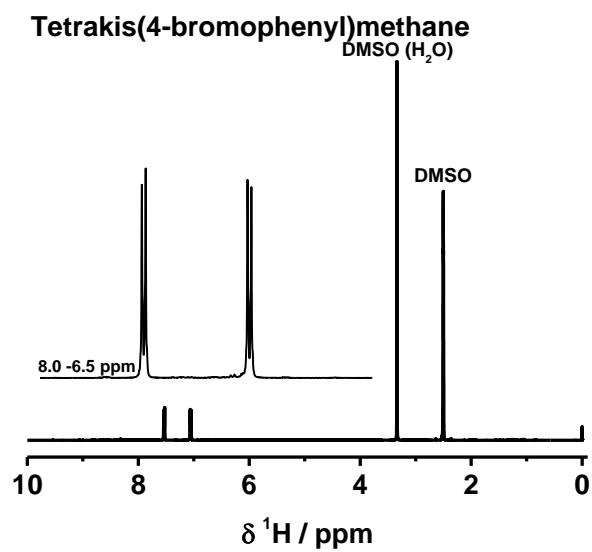


Figure S4: ^1H NMR spectra of Tetrakis(4-bromophenyl)methane.

2.1.1.4 ^{13}C Tetrakis(4-bromophenyl)methane

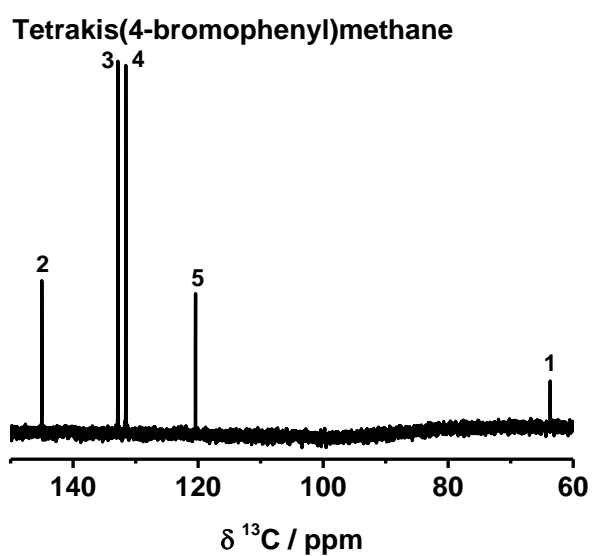


Figure S5: ^{13}C NMR spectrum of Tetrakis(4-bromophenyl)methane.

2.1.2 Infrared spectroscopy

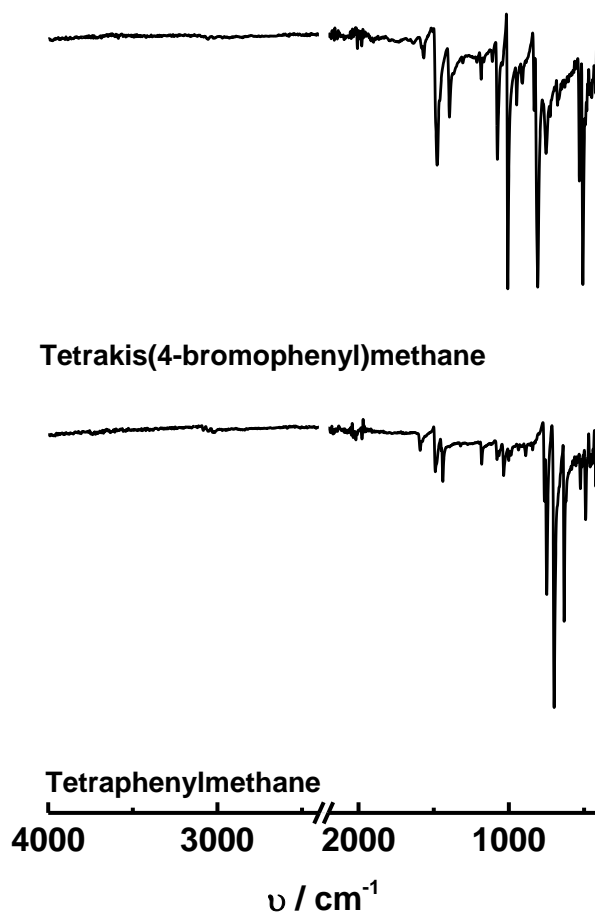


Figure S6: Infrared spectra of tetraphenylmethane and tetrakis(4-bromophenyl)methane.

2.1.3 CHN-Analysis

2.1.3.1 Tetraphenylmethane

Table S3: Results from CHN-analysis of tetraphenylmethane.

TPM	C [%]	H [%]	N [%]
Meas.	91.25	6.544	0.18
Calc.	93.71	6.29	0
Aberration	2.46	0.25	0.18

2.1.3.2 Tetrakis(4-bromophenyl)methane

Table S4: Results from CHN-analysis of tetrakis(4-bromophenyl)methane.

TBPM	C	H	N
Meas.	46.09	2	0.08
Calc.	47.21	2.54	0
Aberration	1.12	0.41	0.08

2.2 Polymer analytics

2.2.1 Solid state NMR

2.2.1.1 ^{13}C _PAF-1

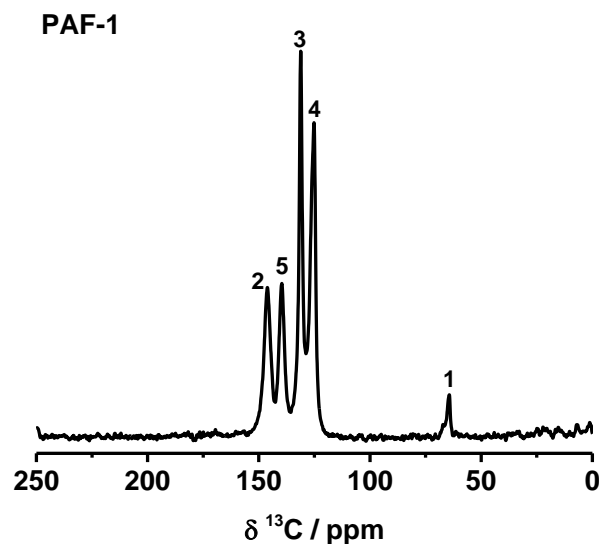


Figure S7: ^{13}C CP MAS NMR spectrum of PAF-1.

Calculation of the crosslinking degree for PAF-1

The resonances of a quantitative MAS single pulse ^{13}C spectrum (Figure S8) were deconvoluted using a pseudo-Voigt lineshape with a 1:1 ratio for the Gaussian and Lorentzian components. For 100 % crosslinking the intensity of C-5 ($I(\text{C-5})$) should equal that of C2 ($I(\text{C-2})$). Based on the reaction mechanism of the used Yamamoto coupling, in case of an incomplete turnover we expect either C-Br moieties (if no reaction occurred) or C-H moieties (if no CC coupling occurred). Both signals are predicted to have ^{13}C chemical shifts around 125 ppm (C-H) and 122 ppm (C-Br). Both resonances are thus superimposed with the signal for C4 and no additional signals are expected. As a consequence, while $I(\text{C-5})$ reduces, $I(\text{C-4})$ is increased. At the same time, $I(\text{C-2})$ should remain unaffected. Thus the intensity ratio $I(\text{C-5}):I(\text{C-2})$ estimated to 0.76(10) is a measure for the degree of crosslinking within the network.

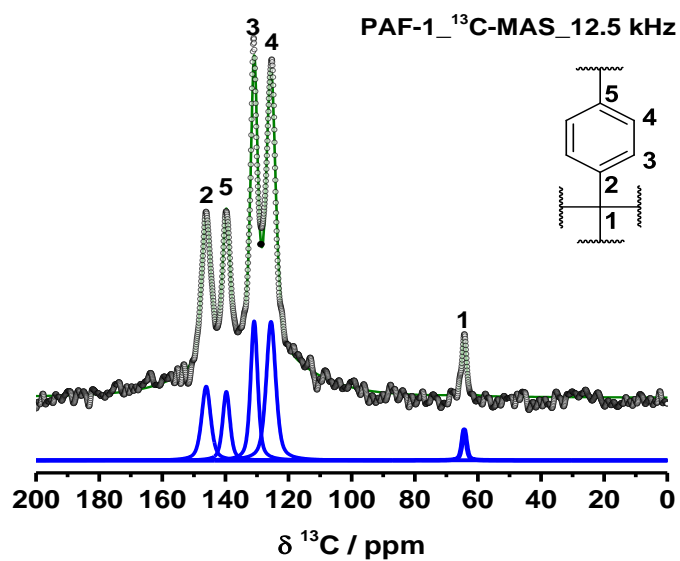


Figure S8: ¹³C MAS onepulse NMR spectrum of PAF-1 for quantitative analysis.

Table 5: Fit parameter derived from the Gauss/Lorentz model based deconvolution of the ¹³C MAS onepulse spectrum of PAF-1 with an overlap of 95.17%.

Sites	2	5	3	4	1
$\delta(\text{iso}) / \text{ppm}$	146.19	139.8	130.9	125.7	64.5
LB / Hz	253.74	203.6	197.8	265.8	124.0
xG/(1-x)L	0.5	0.5	0.5	0.5	0.5
Integral	4.9	3.7	7.2	9.6	1

2.2.1.2 ^{13}C _SPAF-10.5

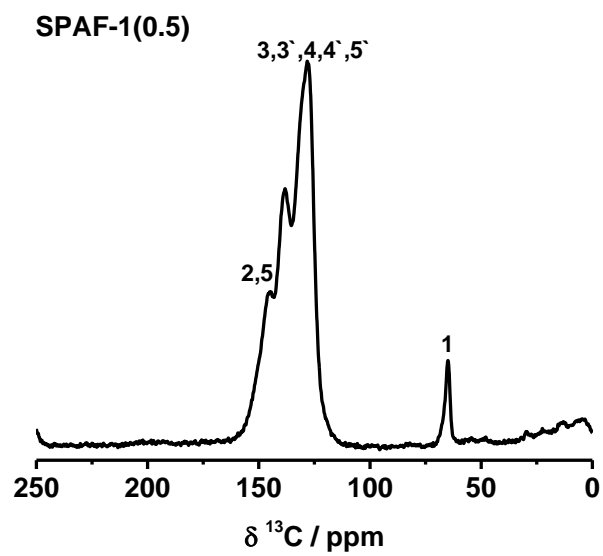


Figure S9: ^{13}C spectrum of SPAF-1(0.5).

2.2.1.3 ^{13}C _SPAF-1(1.25)

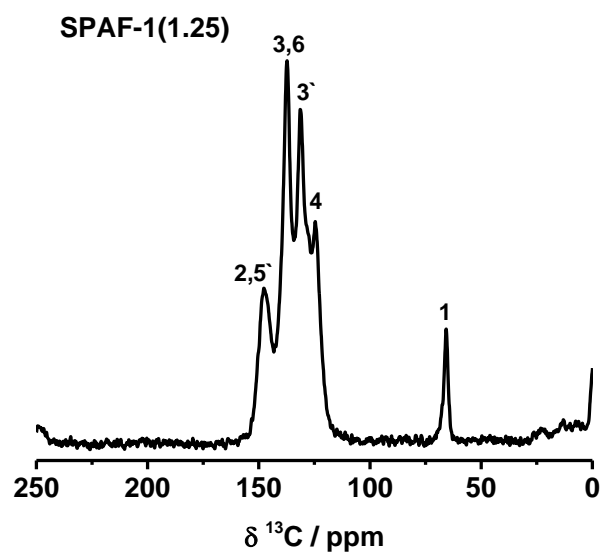


Figure S10: ^{13}C spectrum of SPAF-1(1.25).

2.2.2 Infrared spectroscopy

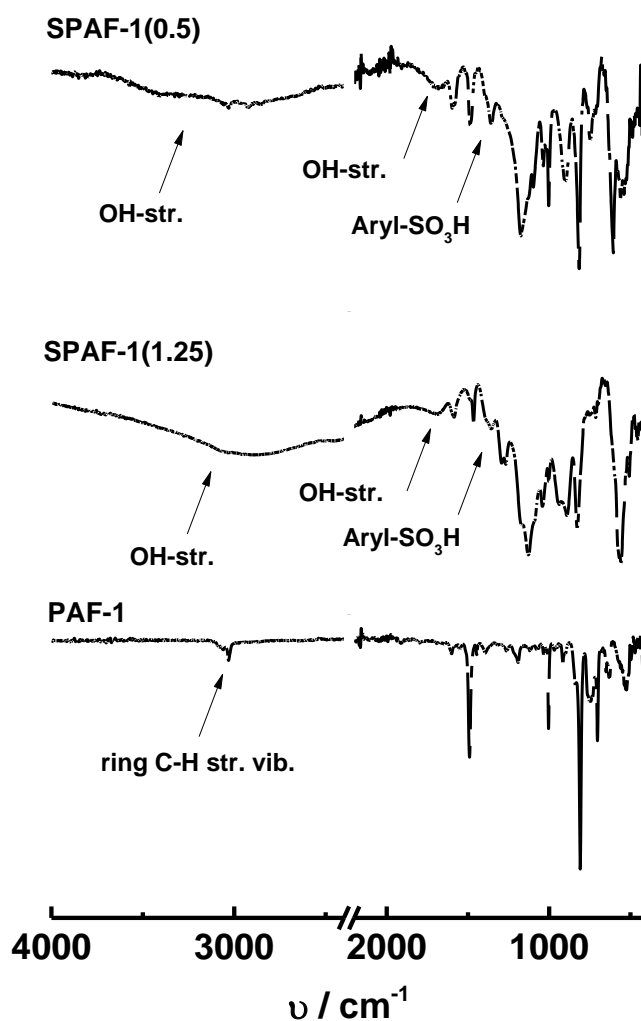


Figure S11: Infrared spectra of PAF-1, SPAF-1(0.5) and SPAF-1(1.25).

2.2.3 CHN-Analysis

2.2.3.1 PAF-1

Table S6: Results from CHN-analysis of PAF-1.

Polymer	C / %	H / %	N / %
PAF-1 _{calc.}	94.90	5.10	0.00
PAF-1 _{meas.}	92.17	5.74	0.63
Deviation	2.73	0.64	0.63

2.2.3.2 SPAF-1(0.5)

Table S7: Results from CHN-analysis of SPAF-1(0.5).

Polymer	C / %	H / %	N / %
SPAF-1(0.5) _{calc}	63.01	3.38	0.00
SPAF-1(0.5) _{meas}	65.47	4.45	0.47
Deviation	2.46	1.07	0.47

2.2.3.3 SPAF-1(1.25)

Table S8: Results from CHN-analysis of SPAF-1(1.25).

Polymer	C / %	H / %	N / %
SPAF-1(1.25) _{calc}	41.9	2.25	0.00
SPAF-1(1.25) _{meas}	41.31	3.71	0.53
Deviation	0.59	1.46	0.53

2.2.4 Gas adsorption analysis – N₂ at 77K

2.2.4.1 PAF-1

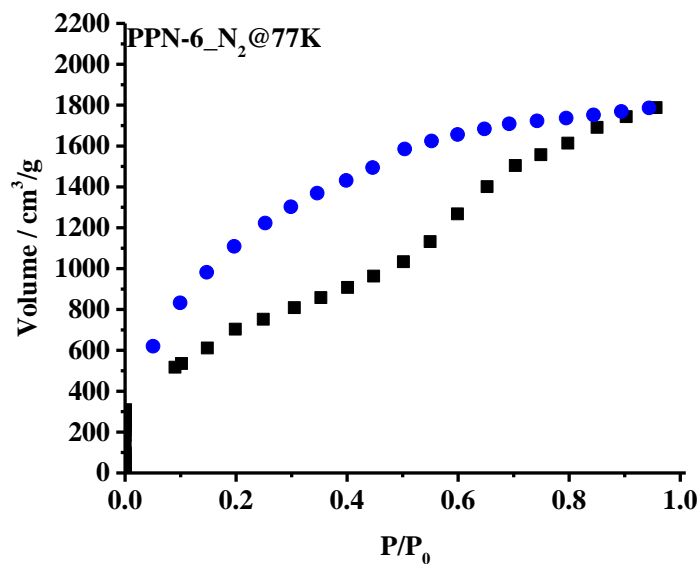


Figure S12: Adsorption isotherm of PAF-1 measured with N₂ at 77 K.

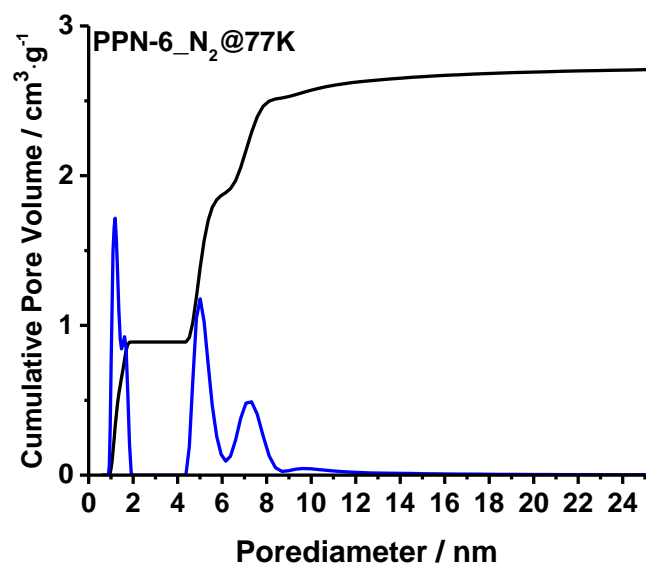


Figure S13: Pore size distribution of PAF-1, calculated from the N₂ at 77 K adsorption isotherm using slit/cylindrical pore QSDFT adsorption branch model.

2.2.4.2 SPAF-1(0.5)

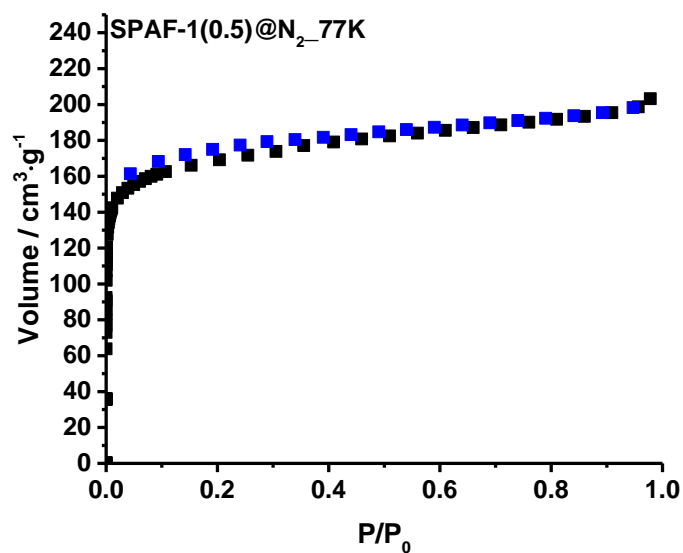


Figure S14: Adsorption isotherm of PAF-1-SO₃H_{solv} measured with N₂ at 77 K.

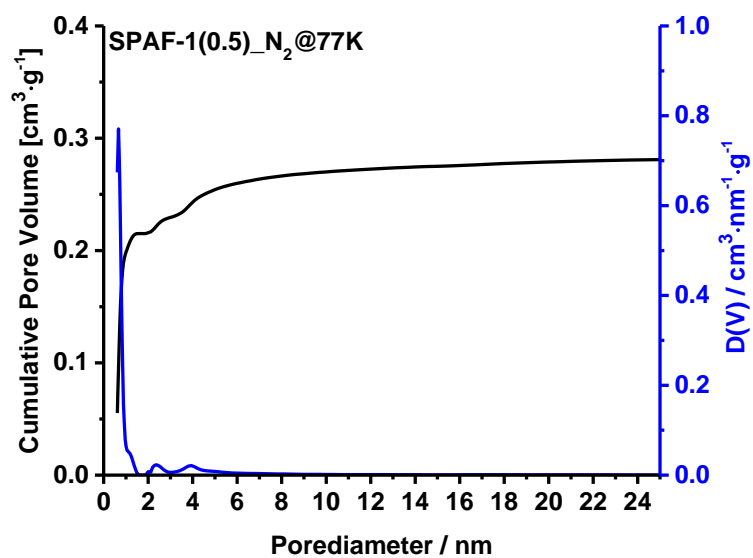


Figure S15: Pore size distribution of SPAF-1(0.5) calculated from the N₂ at 77 K adsorption isotherm using slit/cylindrical pore QSDFT adsorption branch model.

2.2.4.3 SPAF-1(1.25)

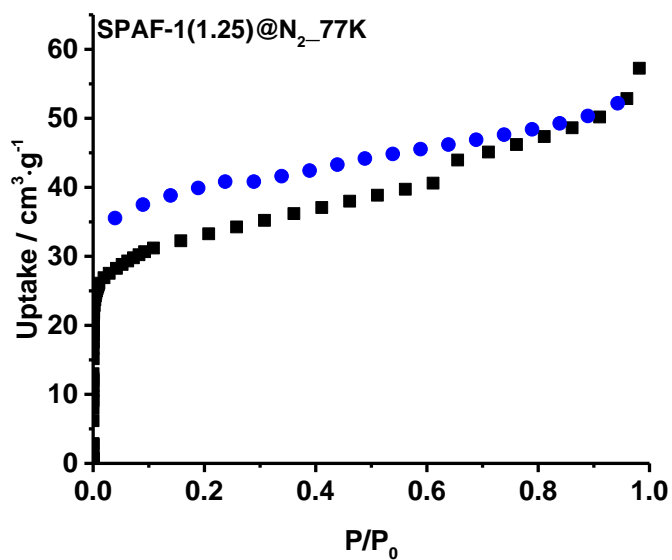


Figure S16: Adsorption isotherm of SPAF-1(1.25) measured with N₂ at 77 K.

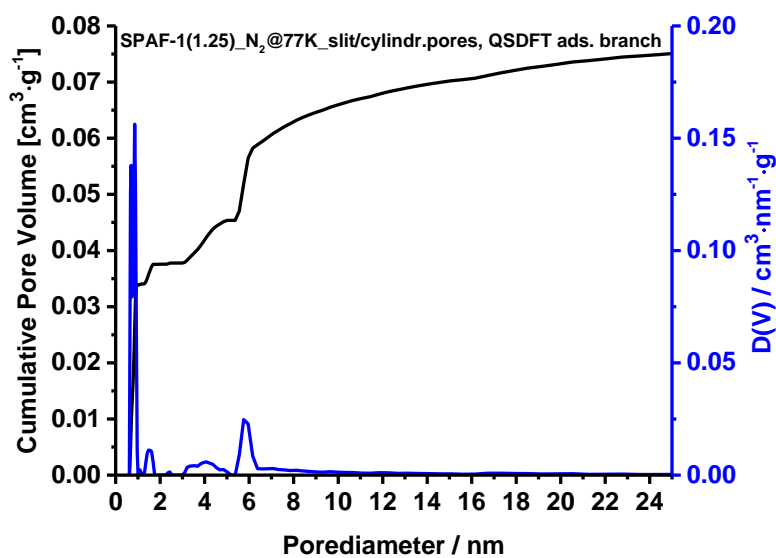


Figure S17: Pore size distribution of SPAF-1(1.25), calculated from the N₂ at 77 K adsorption isotherm using slit/cylindrical pore QSDFT adsorption branch model.

2.2.5 Gas adsorption analysis – CO₂ at 273 K

2.2.5.1 PAF-1

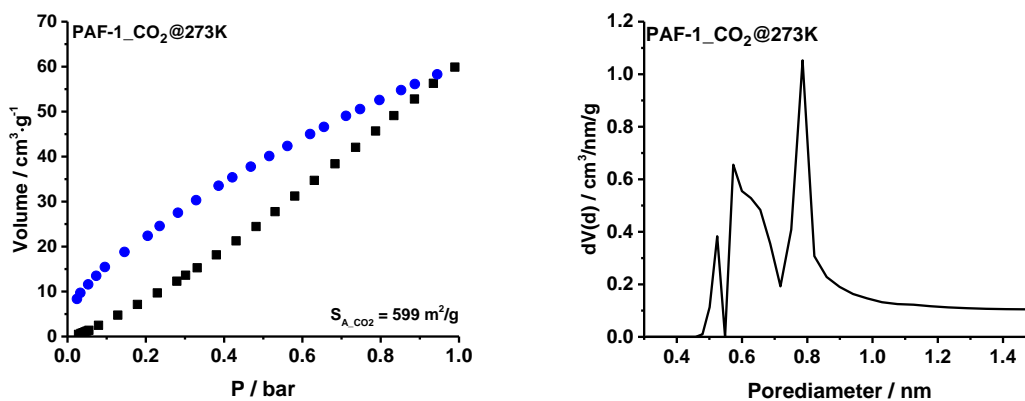


Figure S18: CO₂ Isotherm (left) and pore size distribution (right) of PAF-1. PSD was calculated using CO₂ at 273 K on Carbon NLDFT model.

2.2.5.2 SPAF-1(0.5)

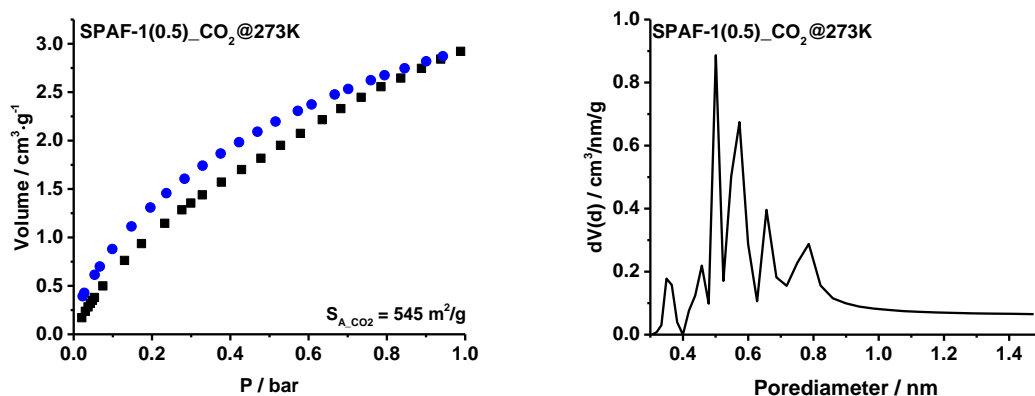


Figure S19: CO₂ Isotherm (left) and pore size distribution (right) of PAF-1-SO₃H_{sol}. PSD was calculated using CO₂ at 273 K on Carbon NLDFT model.

2.2.5.3 SPAF-1(1.25)

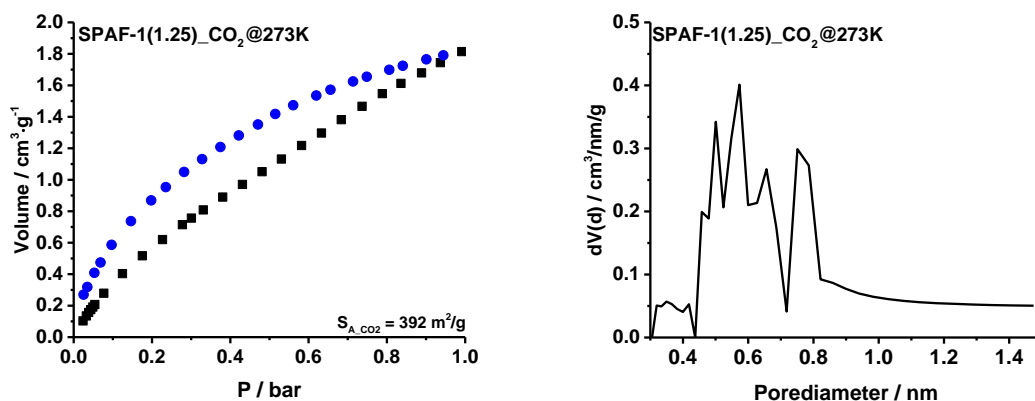


Figure S20: CO₂ Isotherm (left) and pore size distribution (right) of SPAF-1(1.25). PSD was calculated using CO₂ at 273 K on Carbon NLDFT model.

2.2.5.4 Summary of gas sorption analysis

Table S9: Data calculated from N₂ isotherms at 77 K and CO₂ isotherms at 273 K. For calculation the respective BET or DFT kernels were used.

Polymer	$S_{A_BET-N_2} / m^2 \cdot g^{-1}$	$S_{A_DFT-N_2} / m^2 \cdot g^{-1}$	$P_{V_N_2} / cm^3 \cdot g^{-1}$	P_{V_mic} / P_{V_tot}	$S_{A_DFT-CO_2} / m^2 \cdot g^{-1}$	$P_{V_CO_2} / cm^3 \cdot g^{-1}$
PAF-1	2625	2043	2.68	0.33	599	0.234
SPAF-1(0.5)	650	670	0.29	0.75	545	0.177
SPAF-1(1.25)	123	115	0.08	0.47	392	0.132

2.2.6 TGA analysis

2.2.6.1 Stability

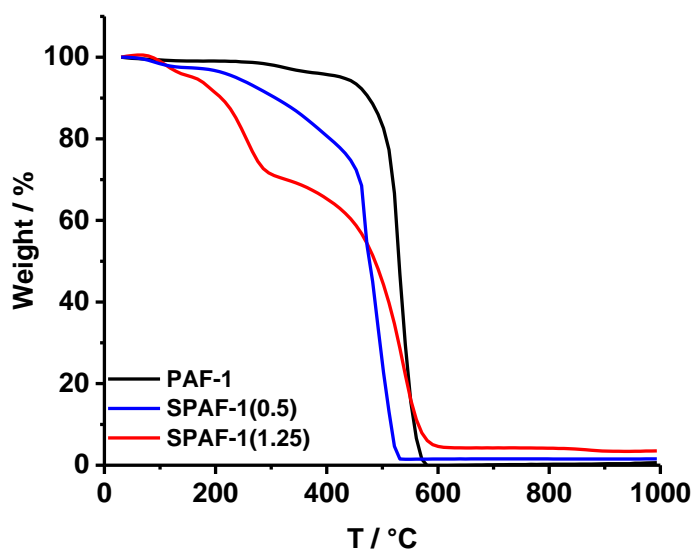


Figure S21: Thermogravimetric data from PAF-1, SPAF-1(1.25) and SPAF-1(0.5), respectively. All Curves were measured under air with a 10 °C / min temperature ramp.

2.2.6.2 Water Uptake

Table S10: Water uptake versus theoretical pore volume for SPAF-1(0.5) and SPAF-1(1.25).

Polymer	Uptake _{H₂O} ^{@100%rH}	P _{V_theoretical} ^{N₂}	Uptk. _{H₂O} /P _{V_theo.}
SPAF-1(0.5)	0.65 cm ³ ·g ⁻¹	0.47 cm ³ ·g ⁻¹	1.38
SPAF-1(1.25)	1.68 cm ³ ·g ⁻¹	0.21 cm ³ ·g ⁻¹	8

2.2.7 UV-Vis spectroscopy

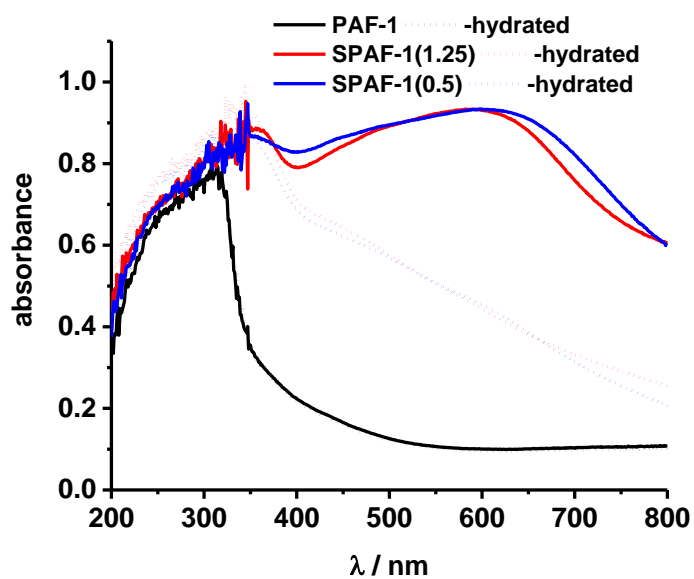


Figure S22: UV-VIS spectra of PAF-1, SPAF-1(1.25) and SPAF-1(0.5), respectively. Full lines show the absorbance of the polymers in the dry state, dashed lines stand for fully hydrated state.

2.2.8 Powder X-ray diffraction

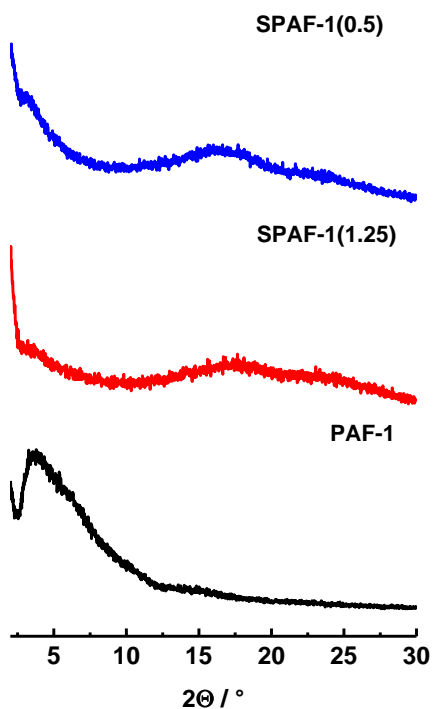


Figure S23: PXRDs of PAF-1, SPAF-1(1.25) and SPAF-1(0.5).

2.2.9 Impedance spectroscopy

2.2.9.1 PAF-1(0.5)

100% rH (H₂O):

Table S11: Temperature dependent resistance and conductivity values of SPAF-1(0.5) at 100 % rH taken from the related Nyquist plots. The data was calculated based on a pellet with $l = 0.25$ cm and $r = 0.4$ cm.

T / °C	T / K	R₂/ Ω	κ / S·cm⁻¹
25	298	505.1	0.00098
33	306	299.1	0.00166
38	311	248	0.00201
42	315	208.3	0.00239
48	321	149.4	0.00333
58	331	115	0.00433
68	341	76.82	0.00648
72	345	43.11	0.01154
78	351	25.42	0.01957

50 % rH (K₂CO₃):

Table S12: Temperature dependent resistance and conductivity values of SPAF-1(0.5) at 50 % rH taken from the related Nyquist plots. The data was calculated based on a pellet with $l = 0.19$ cm and $r = 0.4$ cm.

T / °C	T / K	R₂/ Ω	κ / S·cm⁻¹
22	295	10052	$3.76 \cdot 10^{-5}$
25	298	8707	$4.34 \cdot 10^{-5}$
32	305	7232	$5.23 \cdot 10^{-5}$
37	310	5191	$7.28 \cdot 10^{-5}$
42	315	4340	$8.71 \cdot 10^{-5}$
47	320	3635	$1.04 \cdot 10^{-4}$
52	325	2732	$1.38 \cdot 10^{-4}$
57	330	2198	$1.72 \cdot 10^{-4}$

60	333	1850	$2.04 \cdot 10^{-4}$
68	341	1513	$2.49 \cdot 10^{-4}$
71	344	1341	$2.82 \cdot 10^{-4}$
77	350	1214	$3.11 \cdot 10^{-4}$

30 % rH (H₃C₂OOK):

Table S13: Temperature dependent resistance and conductivity values of SPAF-1(0.5) at 30 % rH taken from the related Nyquist plots. The data was calculated based on a pellet with $l = 0.2$ cm and $r = 0.4$ cm.

T / °C	T / K	R₂ / Ω	κ / S·cm⁻¹
22	295	138830	$2.87 \cdot 10^{-6}$
25	298	110690	$3.59 \cdot 10^{-6}$
30	303	77582	$5.13 \cdot 10^{-6}$
35	308	58635	$6.79 \cdot 10^{-6}$
40	313	46654	$8.53 \cdot 10^{-6}$
45	318	35636	$1.12 \cdot 10^{-5}$
50	323	29521	$1.35 \cdot 10^{-5}$
57	330	24057	$1.65 \cdot 10^{-5}$
63	336	18073	$2.20 \cdot 10^{-5}$
65	338	14929	$2.67 \cdot 10^{-5}$
70	343	11757	$3.38 \cdot 10^{-5}$
75	348	8648	$4.60 \cdot 10^{-5}$
80	353	7375	$5.40 \cdot 10^{-5}$

2.2.9.2 SPAF-1(1.25)

100% rH (H₂O):

Table S14: Temperature dependent resistance and conductivity values of SPAF-1(1.25) taken from the related Nyquist plots. The data was calculated based on a pellet with $l = 0.2$ cm and $r = 0.4$ cm.

T / °C	T / K	R₂ / Ω	κ / S·cm⁻¹
25	298	16.9	0.018
31	304	12.3	0.024
37	310	10.8	0.028
43	316	8.9	0.034
48	321	5.6	0.053
53	326	4.3	0.094
58	331	3.9	0.103
63	336	3.4	0.118
68	341	2.7	0.148
73	346	2.5	0.157
77	350	2.5	0.157

50 % rH (K₂CO₃):

Table S15: Temperature dependent resistance and conductivity values of SPAF-1(0.5) at 50 % rH taken from the related Nyquist plots. The data was calculated based on a pellet with $l = 0.2$ cm and $r = 0.4$ cm.

T / °C	T / K	R₂ / Ω	κ / S·cm⁻¹
21	294	12269	$4.05 \cdot 10^{-5}$
25	298	8378	$5.94 \cdot 10^{-5}$
30	303	4473	$1.11 \cdot 10^{-4}$
35	308	2545	$1.95 \cdot 10^{-4}$
42	315	1384	$3.59 \cdot 10^{-4}$
48	321	1066	$4.67 \cdot 10^{-4}$
53	326	829	$5.99 \cdot 10^{-4}$

58	331	654	$7.60 \cdot 10^{-4}$
62	335	564	$8.82 \cdot 10^{-4}$
66	339	590	$8.43 \cdot 10^{-4}$
72	345	450	0.00111
77	350	389	0.00128
80	353	386	0.00129

30 % rH (H₃C₂OOK):

Table S16: Temperature dependent resistance and conductivity values of SPAF-1(0.5) at 30 % rH taken from the related Nyquist plots. The data was calculated based on a pellet with $l = 0.18$ cm and $r = 0.4$ cm.

T / °C	T / K	R₂ / Ω	κ / S·cm⁻¹
22	295	84342	$4.24 \cdot 10^{-6}$
25	298	73798	$4.85 \cdot 10^{-6}$
30	303	56344	$6.35 \cdot 10^{-6}$
35	308	40898	$8.77 \cdot 10^{-6}$
40	313	29112	$1.23 \cdot 10^{-5}$
45	318	20231	$1.77 \cdot 10^{-5}$
50	323	13869	$2.58 \cdot 10^{-5}$
55	328	11939	$2.99 \cdot 10^{-5}$
62	335	8364	$4.28 \cdot 10^{-5}$
66	339	7245	$4.94 \cdot 10^{-5}$
70	343	5509	$6.49 \cdot 10^{-5}$
75	348	4221	$8.48 \cdot 10^{-5}$
80	353	3366	$1.06 \cdot 10^{-4}$

2.2.10 Differential scanning calorimetry

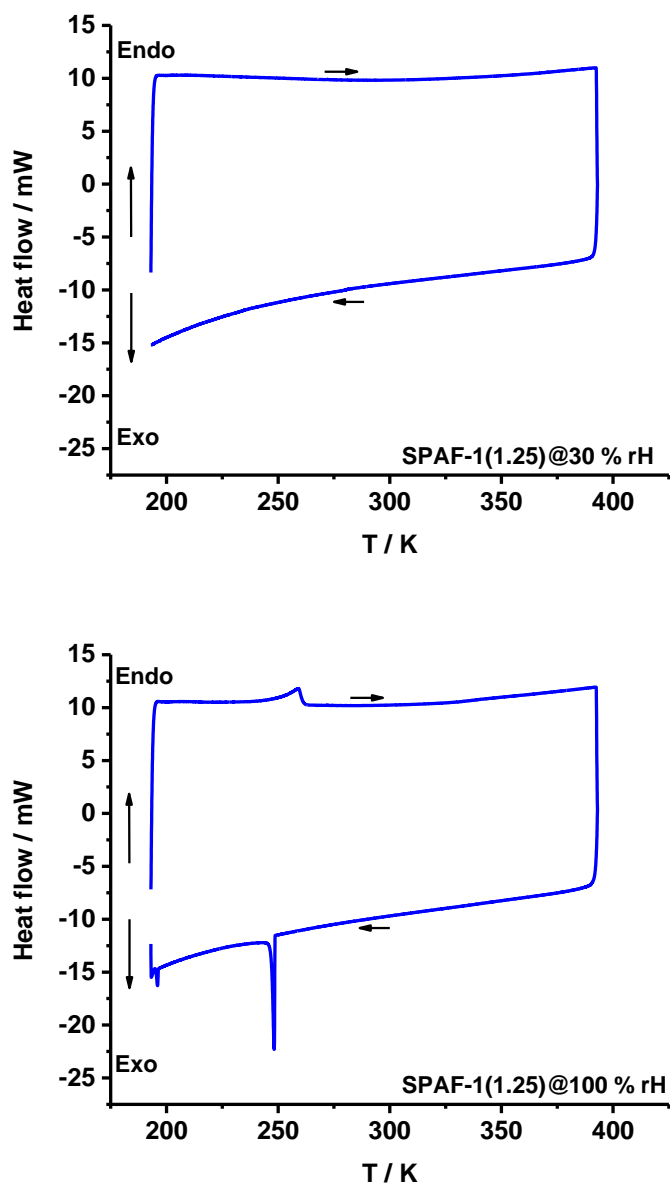


Figure S24: DSC curves for SPAF-1(1.25) hydrated at 30 % (top) and 100 % rH (bottom).

For SPAF-1(1.25) saturated for 100 %rH (Figure S24 bottom) an endothermic melting peak at around -25 °C with an area equivalent to 0.35 J was observed. With a melting enthalpy (ΔH_m) for water of 333.5 J/g, this corresponds to 0.06 mmol water. In contrast, TG measurements revealed a total amount of 0.23 mmol water to be adsorbed within the network. Thus, only 25 % of the incorporated water is stored in mesopores, while 85 % is located in micropores.

2.2.11 Energy dispersive X-ray spectroscopy

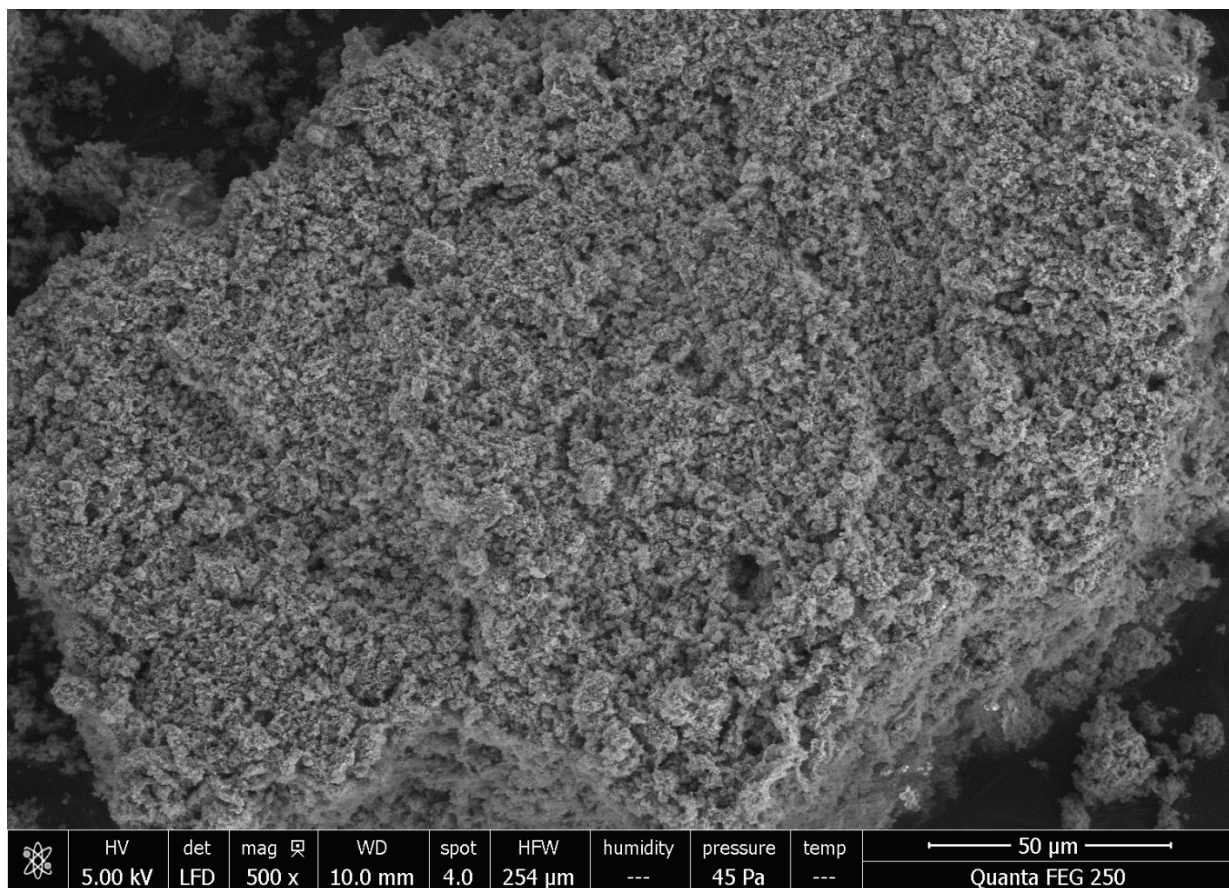


Figure S25: REM image of Na-SPAF-1(1.25).

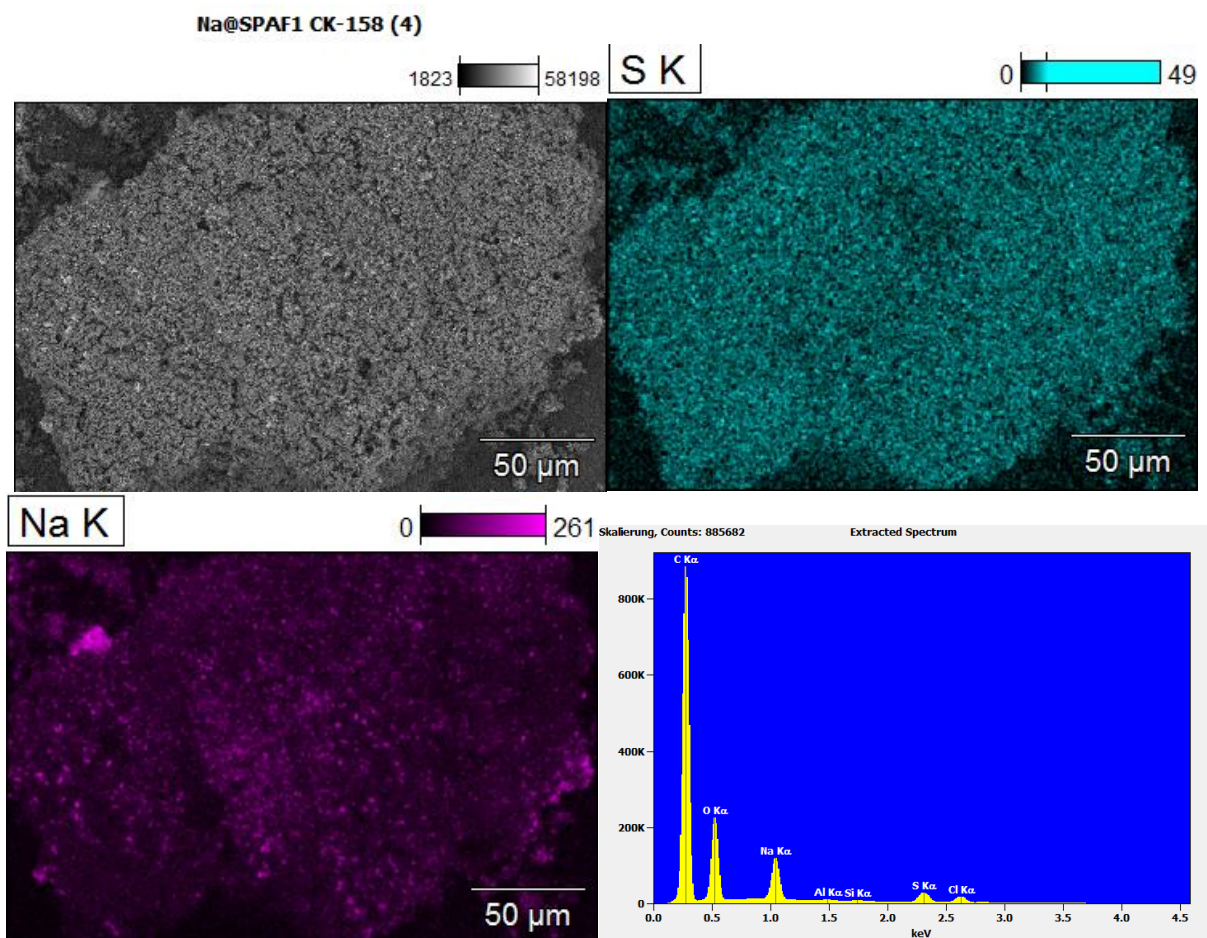
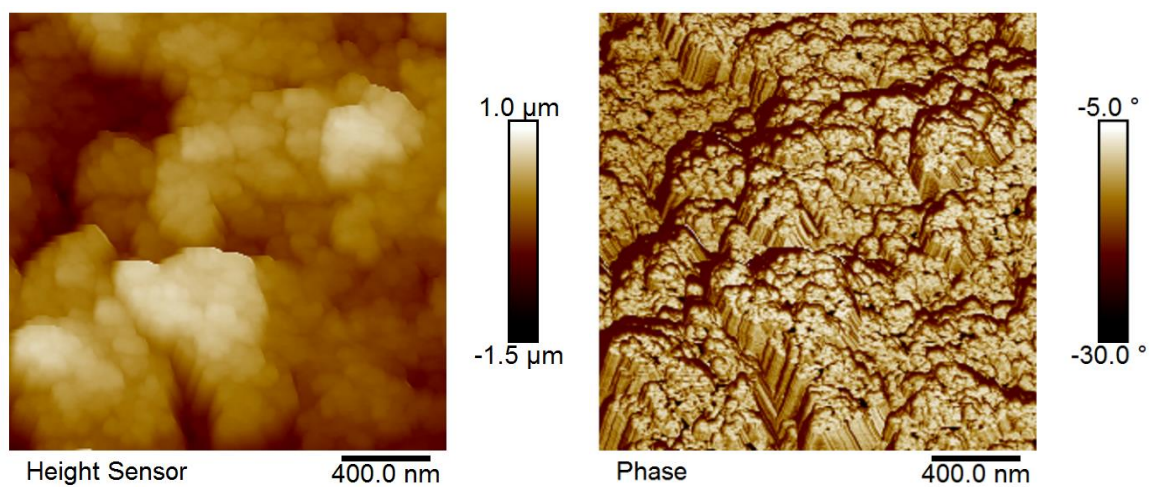


Figure S26: EDX spectra of Na-SPAF-1(1.25) without coloration, blue colored sulfur distribution, violet colored sodium distribution.

2.2.12 Atomic force microscopy



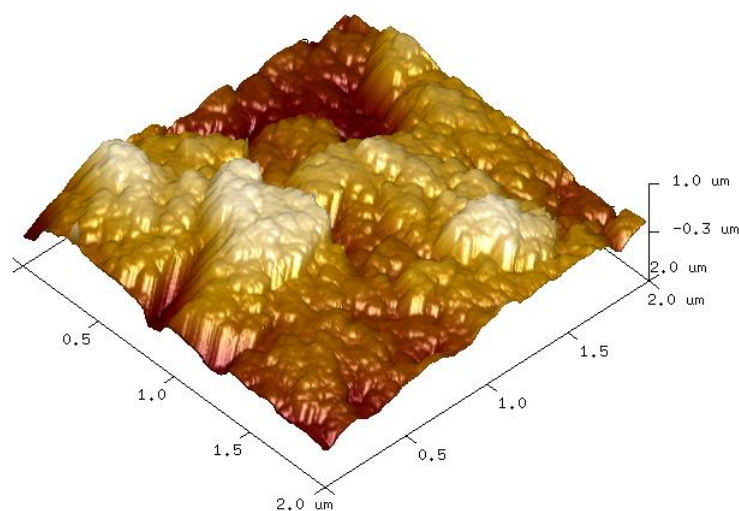


Figure S27: Height image (top, left) and corresponding phase image (top, right) as well as 3D surface mapping (bottom) of a pelletized (SPAF-1.25) sample, derived from AFM measurements.

3. Literature

- [1] B. M. Fung, A. K. Khitrin, K. Ermolaev, *J. Magn. Reson.* **2000**, *142*, 97–101.
- [2] W. Lu, D. Yuan, D. Zhao, C. I. Schilling, O. Plietzsch, T. Muller, S. Bräse, J. Guenther, J. Blümel, R. Krishna, et al., *Chem. Mater.* **2010**, *22*, 5964–5972.
- [3] Y. He, S. Xiang, B. Chen, *J. Am. Chem. Soc.* **2011**, *133*, 14570–3.
- [4] W. Lu, D. Yuan, J. Sculley, D. Zhao, R. Krishna, H.-C. Zhou, *J. Am. Chem. Soc.* **2011**, *133*, 18126–9.
- [5] S. Kittaka, S. Takahara, H. Matsumoto, Y. Wada, T. J. Satoh, T. Yamaguchi, *J. Chem. Phys.* **2013**, *138*, 204714.
- [6] N. Walsby, S. Hietala, S. L. Maunu, F. Sundholm, T. Kallio, G. Sundholm, *J. Appl. Polym. Sci.* **2002**, *86*, 33–42.